

# NETWORK TOMOGRAPHY-BASED TRACKING FOR INTRACELLULAR TRAFFIC ANALYSIS IN FLUORESCENCE MICROSCOPY IMAGING

Thierry Pécot<sup>1,2</sup>, Charles Kervrann<sup>1,2</sup> and Patrick Boutheymy<sup>1</sup>

<sup>1</sup>IRISA/INRIA, Campus universitaire de Beaulieu, F-35042 Rennes, France

<sup>2</sup>INRA, UR341 Mathématiques et Informatique Appliquées, F-78352 Jouy-en-Josas

**Keywords:** Object tracking, fluorescence microscopy, network tomography, Voronoi diagram, trafficking, membrane transport.

**Abstract:** Determination of the sub-cellular localization and dynamics of any proteins is an important step towards the understanding of multi-molecular complexes in a cellular context. Green Fluorescent Protein (GFP)-tagging and time-lapse fluorescence microscopy allows to acquire multidimensional data on rapid cellular activities, and then make possible the analysis of proteins of interest. Consequently, novel techniques of image analysis are needed to quantify dynamics of biological processes observed in such image sequences. In biological trafficking analysis, the previous tracking methods do not manage when many small and poorly distinguishable objects interact. Nevertheless, an another way of tracking that usually consists in determining the full trajectories of all the objects, can be more relevant. General information about the traffic like the regions of origin and destination of the moving objects represent interesting features for analysis. In this paper, we propose to estimate the paths (regions of origin and destination) used by the objects of interest, and the proportions of moving objects for each path. This can be accomplished by exploiting the recent advances in Network Tomography (NT) commonly used in network communications. This idea is demonstrated on real image sequences for the Rab6 protein, a GTPase involved in the regulation of intracellular membrane trafficking.

## 1 INTRODUCTION

Small GTPases play a key role in many aspects of cell biology: control of cell growth and differentiation, regulation of cell adhesion and cell movement, organization of the actin cytoskeleton, and regulation of intracellular vesicular transport. The small GTPases Rab proteins are important regulators of trafficking within the membrane. Each member of this family (60 described in human cells) exists under different dynamic states in the cell: *i*) diffusion in the cytosol; *ii*) exchanges between the cytosol and the membranes; *iii*) vesicular transport. The Rab protein family plays an essential role in the dynamics of the transport vesicles and their targeting/anchoring with the acceptor membranes. Studying the role of Rab proteins inside multiprotein complexes is then fundamental to deeply understand the molecular mechanisms responsible for membrane transport and for the maintenance of the integrity and global architecture of the cell, in space and time.

Rab6 is located on the Golgi Apparatus membranes and the trans-Golgi network membranes. It is

involved in a retrograde transport from the Golgi Apparatus to the Endoplasmic Reticulum. When Rab6 proteins embedded into vesicles are marked with GFP (Green Fluorescence Protein), they appear on the image sequence as blobs heterogeneously moving along the microtubule network. The study of the membrane trafficking by measuring the activity of small transport vesicles from donor to acceptor compartments within the cell thanks to image analysis techniques is challenging.

Rab6 trafficking is really hard to analyse as it is composed of several hundreds similar objects that are moving with variable velocities. The most commonly used tracking concept is the connexionist approach (Anderson et al., 1992; Sbalzarini and Koumoutsakos, 2005; Racine et al., 2006) consisting in detecting particles independently in each frame in a first time, and then linking the detected objects over time. But, measurements from clutter and multiple objects make the data association problem very hard to compute. From now, data association even combined with sophisticated particle filtering techniques (Smal et al., 2007) or graph-theory based methods

(Thomann et al., 2003) are problematic to track several hundreds of similar objects with a high reliability.

Deterministic approaches have also been explored. (Sibarita et al., 2006) exploits the fact that vesicles are moving along the microtubule network, and thus follow the same paths. Kymograms are used for analysing the time intensity profile of the given paths. The main limitation of the kymogram-based method is that each path is independently supervised. Another line of work consists in detecting changes in the temporal signal for a set of pixels (Bechar and Trubuil, 2006). By grouping similar temporal profiles, dynamics of vesicles can be better described.

In this paper, we propose to get around the difficult problem of data association by using an original statistical approach. The aim is to apply the Network Tomography (NT) concept to real image sequences, which is challenging for several reasons described below. Accordingly, we need to construct a graph and to propose a method to measure the activity on edges, according to the NT approach (Vardi, 1996). This is the main contribution of this paper. The NT-based approach, already applied in video surveillance (Santini, 2000; Boyd et al., 1999), allows us to track objects but only requires the detection of the objects when they move from one region to another. The estimated variables give only a general aspect of the whole traffic, but the data association, usually complex, is not needed. In this paper, we propose to adapt this NT concept to the estimation of trajectories of vesicles since it can be motivated by biological analyses. The number of vesicles that pass through each transition of the graph is estimated by solving an underconstrained optimization problem. We will demonstrate that this method is suited for understanding membrane transport. The paper is organized as follows: in Section 2, we propose to partition the image into regions of interest, and we estimate the number of moving vesicles on edges at each time step. Then, this estimation is tested on simulations. In Section 3, we estimate the regions of origin and destination for the vesicles, and these estimations are tested on a real image sequence in Section 4. Finally, we present a conclusion and the perspectives in Section 5.

## 2 MEASUREMENTS ON EDGES

In (Pécot et al., 2007), the idea was to extract the microtubule network, and to determine the origin and destination regions for the vesicles, and the crossings of different microtubules, all labeled as vertices in the graph. Vertices and edges (links between vertices) define the graph  $\mathcal{G} = \{E, V\}$ , and the activ-

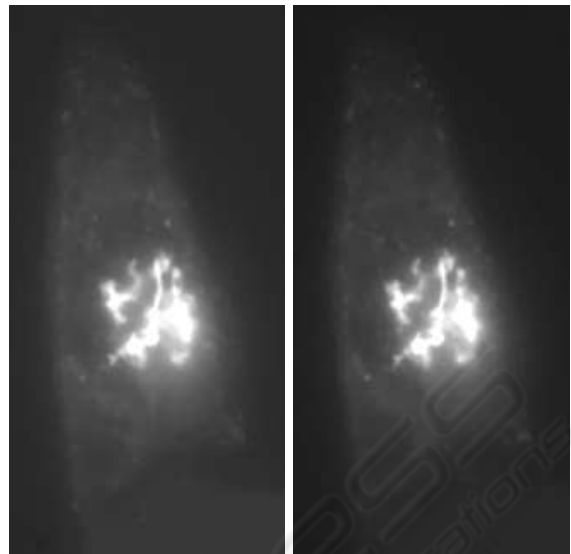


Figure 1: Images extracted from a microscopic sequence using a fast 4D deconvolution (wide-field) process at two time steps.

ity measurements on edges correspond to the observations required to apply the NT-based approach, which amounts to estimating the origin-destination (OD) pairs for the vesicles. In other words, our goal is to determine the different paths used by the vesicles from the donor compartment to the acceptor compartment, and the proportions of vesicles for each path. However, the extraction of the microtubule network is really hard to compute, since very complex with limited spatial resolution. So we prefer to partition the image into regions and to represent the relationships between regions using a graph.

### 2.1 Image Partitionning

The Maximum Intensity Projection (MIP) map in the direction of time axis is a precious key for the partitionning of a cell compartment. Indeed, the likely regions of origin or destination appear as brighter spots in the MIP map because vesicles are temporally stocked in these areas. For illustration, the MIP map extracted from the image sequence shown in Fig. 1 is given in Fig. 2. It is established that the Golgi Apparatus is the main origin region for Rab6 protein. This region appears as a very bright region in the MIP map as shown in Fig. 2. A possible image partitionning consists in dividing the image into Voronoi cells as in (Boyd et al., 1999). The Voronoi cells are further assumed to be the OD regions observed in the MIP map. It is also possible to compute a Voronoi diagram at a finest spatial resolution including crossings as relevant features for traffic analysis.

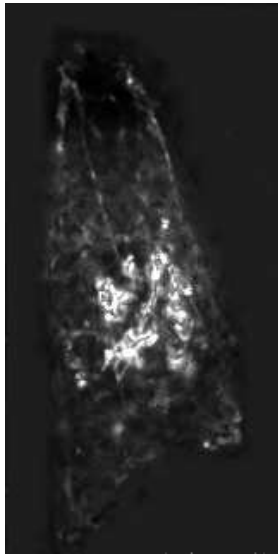


Figure 2: MIP map extracted from the image sequence shown in Fig. 1.

In order to partition the regions of interest within the cell, the expert can also manually define the centers of the Voronoi diagram if required. This diagram is then computed using the *qhull* library (Barber et al., 1996). A segmentation for the cell observed in the image sequence of Fig. 1 is typically illustrated in Fig. 3 where the centers appear in green and the different regions appear in red, while the MIP map is depicted in the background. In this figure, the centers were fixed to represent the Golgi Apparatus, and the three possible end-points of the cell.

The Voronoi diagram is also described by an adjacency graph (Fig. 3, right) and then consistent with the NT concept used for tracking. The different Voronoi cells represent the set of vertices  $V$  while the boundaries between the cells represent the set of edges  $E$ . We introduce two edges between two neighbouring cells in order to analyse trafficking in both directions.

Given the graph  $G$ , the next step consists in extracting the data to apply the NT approach, i.e. estimating the number of vesicles that move from one Voronoi cell to another one during the whole image sequence.

## 2.2 Temporal Estimation of the Number of Moving Vesicles

We want to know exactly how many vesicles are moving from one Voronoi cell to another one at each time step. Our idea is to compute the difference of the number of vesicles observed at two consecutive time

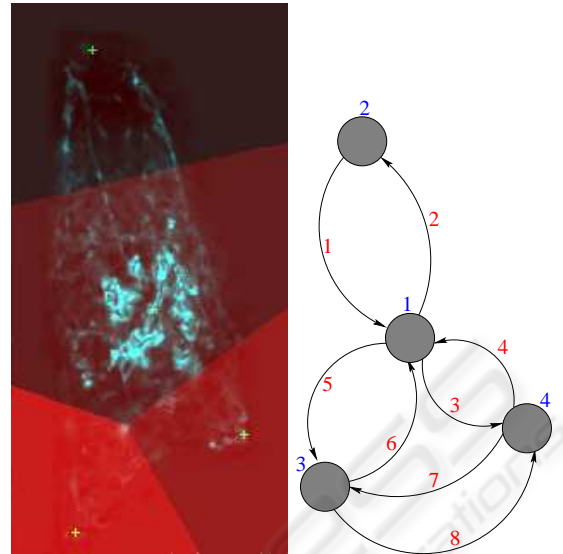


Figure 3: Left: partition of the compartment and surroundings observed in the image sequence shown in Fig. 1 by using a Voronoi decomposition. The different regions appear in red, their centers are labeled in green, and the MIP map is in the background; right: the corresponding graph; the vertex numbers are labeled in blue, while the edge numbers are labeled in red.

steps in each neighbouring region, and then to infer the exact number of vesicles that crosses each common boundary. Nevertheless, computing the difference of vesicles in each region involves image segmentation, a hard task since many similar objects overlap. By applying NT, we circumvent the problem since a crude partition of the image is only needed. In what follows, we assume that the level of fluorescence is proportional to the number of Rab6 proteins at each pixel. So the difference of image intensity at two time steps represents the difference of the number of Rab6 proteins in each region. In practice, the background corresponding to the Golgi apparatus and to the cytosol diffusion is first removed during a preprocessing step (Boulanger et al., 2006) for better performance. We illustrate this concept on a simple example explained below.

We consider the fluorescence exchanges at the vertex 1 in the graph shown in Fig. 3. Let  $Z_{v,t}$  be the total amount of fluorescence in the complete Voronoi region corresponding to the vertex  $v$  at time  $t$ , and let  $Y_{e,t}$  be the level of fluorescence to be determined on edge  $e$  at time  $t$ :

$$Z_{1,t+1} - Z_{1,t} = Y_{1,t+1} - Y_{2,t+1} + Y_{4,t+1} - Y_{3,t+1} + Y_{6,t+1} - Y_{5,t+1}.$$

This equation can be extended to all vertices: let  $\Delta Z$  be the  $n \times t$  matrix corresponding to the difference of

Table 1: Definition of the matrix  $\mathbf{M}$  corresponding to the graph shown in Fig. 3.

edges	vertices			
	1	2	3	4
1	1	-1	0	0
2	-1	1	0	0
3	-1	0	0	1
4	1	0	0	-1
5	-1	0	1	0
6	1	0	-1	0

fluorescence in each region between two consecutive time steps, with  $n$  the number of regions and  $t$  the number of images in the sequence. Let  $\mathbf{Y}$  be the  $r \times t$  matrix representing the level of fluorescence that fluctuates from one region to another at each time, with  $r$  denoting the number of edges. We define  $\mathbf{M}$  as the so-called ‘‘neighbourhood  $n \times r$  matrix’’ composed of ternary elements  $m = \{-1, 0, 1\}$  that links the regions according to the neighbourhood relationships. For example, in Fig. 3,  $\mathbf{M}$  is defined as shown in Tab. 1. Then, we have:

$$\Delta\mathbf{Z} = \mathbf{M}\mathbf{Y} \quad (1)$$

Our aim is to estimate  $\mathbf{Y}$  with  $r > n$  given  $\Delta\mathbf{Z}$ , so to solve an under-constrained problem. Additional constraints are necessary for solving (1). First, we assume that all the components of  $\mathbf{Y}$  are positive since the edges are unidirectional. In addition, the  $\Delta\mathbf{Z}$  rows are assumed to be i.i.d., and we naturally choose the  $\mathcal{L}^2$  distance. Finally, we propose to solve the following optimization problem:

$$\hat{\mathbf{Y}} = \min_{\mathbf{Y}} \|\Delta\mathbf{Z} - \mathbf{M}\mathbf{Y}\|^2 \text{ subject to } \mathbf{Y} \geq \mathbf{0}.$$

This optimization problem leads to an estimation of  $\mathbf{Y}$ . To improve the solution, we also introduce an additional constraint based on the idea of *parsimony* (see (Tibshirani, 1996; Candes and Tao, 2007)). Actually, each row of  $\hat{\mathbf{Y}}$  corresponds to fluorescence exchanges on edges during the whole image sequence. In what follows, we want to check if the estimation of  $\mathbf{Y}$  is improved when the traffic on some edges is removed, especially on edges for which a very low traffic is observed. Accordingly,  $\mathbf{Y}$  is split into positive rows  $\mathbf{Y}_l$  and rows with zero values  $\mathbf{Y}_{n-l}$ . The minimization can be then modified as follows:

$$(\hat{l}, \hat{\mathbf{Y}}) = \min_{l, \mathbf{Y}_l} \|\Delta\mathbf{Z} - \mathbf{M}_l \mathbf{Y}_l\|^2 + \rho l, \text{ subject to } \mathbf{Y} \geq \mathbf{0},$$

where the second term encourages the selection of few edges with  $l$  denoting the number of non-zero rows in  $\mathbf{Y}$ ,  $\rho$  a balance term,  $\mathbf{Y}_l$  the  $(r-l) \times t$  matrix

corresponding to  $\mathbf{Y}$  restricted to rows with significant measurements (non zero),  $\mathbf{M}_l$  the neighbourhood matrix that matches  $\mathbf{Y}_l$ , and  $\Delta\mathbf{Z}$  denoting the difference of fluorescence in each region between two consecutive time steps.

In practice, we propose the following *greedy algorithm* for minimization:

1. compute  $\hat{\mathbf{Y}}_l = \min_{\mathbf{Y}_l \geq \mathbf{0}} \|\Delta\mathbf{Z} - \mathbf{M}_l \mathbf{Y}_l\|^2$ ,
2. compute  $e = \|\Delta\mathbf{Z} - \mathbf{M}_l \hat{\mathbf{Y}}_l\|^2 + \rho l$ ,
3. remove the row  $l'$  in  $\hat{\mathbf{Y}}_l$  that contains the higher number of 0 values,
4. update the matrices  $\mathbf{Y}'$  and  $\mathbf{M}'$  with  $(l-1)$  components,
5. compute  $\hat{\mathbf{Y}}' = \min_{\mathbf{Y}' \geq \mathbf{0}} \|\Delta\mathbf{Z} - \mathbf{M}' \mathbf{Y}'\|^2$ ,
6. compute  $e' = \|\Delta\mathbf{Z} - \mathbf{M}' \hat{\mathbf{Y}}'\|^2 + \rho(l-1)$ ,
7. accept  $\hat{\mathbf{Y}} = \hat{\mathbf{Y}}'$  if  $e' < e$ ,
8. if all rows were considered, stop the procedure, else go back to step 2.

Finally, depending on the microtubule network topology and the related Voronoi diagram, the expert can also forbid the fluorescence transfer between several regions if required. This option is explained in the next section.

### 2.3 Traffic Partially Known

Biological motivations, confirmed by the MIP map, can be exploited to prevent the displacements of vesicles from one region to another one. This can be performed by modifying the neighbourhood matrix  $\mathbf{M}$ . For instance, in Fig. 3, we assume that the expert knows that no vesicle is moving between region 1 and region 2. The matrix is therefore modified accordingly as

$$\begin{aligned} \mathbf{M}(:, 1) &= 0, \text{ and} \\ \mathbf{M}(:, 2) &= 0, \end{aligned}$$

with  $\mathbf{M}(:, 1) = \{\mathbf{M}(1, 1); \mathbf{M}(2, 1); \dots; \mathbf{M}(n, 1)\}$ . For the expert, this flexibility can be appropriate for real applications where interactions with the image is required, as demonstrated in our experiments.

### 2.4 Experiments

In this section, we propose a first set of experiments to evaluate the performance of the estimation procedure, to be exploited in the NT approach described in Section 3. In this experiment, the vesicles at the origin and destination regions are stocked, to take into account the difference of fluorescence.

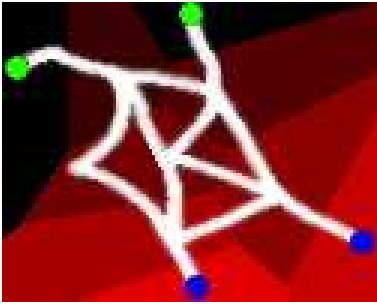


Figure 4: Network used for the first simulation. The microtubule network appears in white, the Voronoi cells are in red, the origin regions are labeled in green, and the destination regions are labeled in blue.

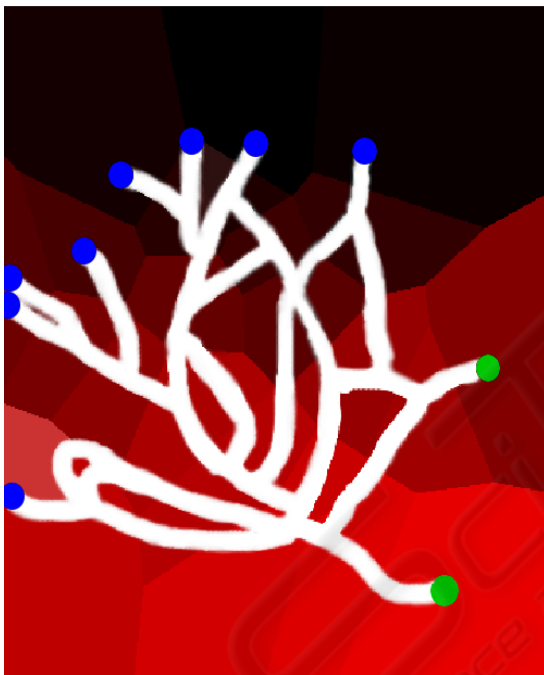


Figure 5: Network used for the second simulation. The microtubule network appears in white, the Voronoi cells are in red, the origin regions are labeled in green, and the destination regions are labeled in blue.

Table 2: Evaluation of the estimation of the traffic from the simulated network shown in Fig. 4.

Temporal tolerances	0	1	2	3
<i>without greedy algorithm</i>				
PFA	36%	9%	5%	4%
PFN	36%	9%	5%	4%
PGD	64%	91%	95%	96%
<i>with greedy algorithm</i>				
PFA	34%	6%	2%	1%
PFN	34%	6%	2%	2%
PGD	65%	94%	98%	99%

Table 3: Evaluation of the estimation of the traffic from the simulated network shown in Fig. 5.

Temporal tolerances	0	1	2	3
<i>without greedy algorithm</i>				
PFA	39%	9%	5%	5%
PFN	39%	11%	7%	7%
PGD	61%	89%	93%	93%
<i>with greedy algorithm</i>				
PFA	35%	5%	1%	1%
PFN	37%	8%	4%	4%
PGD	63%	92%	96%	96%

Two sequences are simulated based on the networks shown in Figs. 4 and 5, where the network appears in white, the Voronoi cells in red, the origin regions in green and the destination regions in blue. The simulations correspond to sequences of 1000 images, showing 2000 moving vesicles.

The performance of our estimation procedure described in Section 2.2 are measured using three criteria:

$$\text{PFA} = \frac{\text{number of false detections}}{\text{total real number of detections}},$$

$$\text{PFN} = \frac{\text{number of true detections not effected}}{\text{total real number of detections}},$$

$$\text{PGD} = \frac{\text{number of good detections}}{\text{total real number of detections}},$$

where PFA denotes the Probability of False Alarms, PFN the Probability of False Negatives, and PGD the Probability of Good Detections.

A slight temporal shifting between the estimation results and the "ground truth" is observed. That is why the results are presented with different temporal tolerances. For instance, a temporal tolerance equal to  $\delta t$  means that the estimation results are compared with a shifting in  $[-\delta t, \dots, \delta t]$  to the ground truth. The temporal estimations of the number of moving vesicles in the simulations based on the networks shown in Figs. 4 and 5 are given in Tabs. 2 and 3. In these tables, the results obtained are shown with and without using the *greedy algorithm*.

Clearly, with a slight temporal tolerance, the estimated results are very close to the "ground truth". In addition, it worth noting that we only use temporal averages for NT, so the shifting will not be crucial for OD pairs estimation. Moreover, it is also confirmed that the *greedy algorithm* significantly improves the estimation results.

### 3 NETWORK TOMOGRAPHY

As explained in Section 2.1 and illustrated in Fig. 3, a region within the cell (e.g. compartment) can be represented by a graph corresponding to a Voronoi diagram, where the centers of the Voronoi cells correspond to regions of interest. The graph  $\mathcal{G}(E, V)$  is defined by  $n$  vertices and  $r$  edges, where  $E$  denotes the set of edges, and  $V$  the set of vertices. A connection between two vertices is also called a path, and each path consists of one or more edges. In the NT-based approach, the data is the number of objects detected as going from one vertex to another vertex in the graph. Based on these measurements, the new goal is to estimate how many vesicles coming from an origin vertex go to a destination vertex along a path, in the set of all possible OD pairs in the graph, that is  $c = n(n-1)$  OD pairs. This problem is then similar to determine the source-destination traffick based on link measurements in computer networks (Vardi, 1996). In this approach, it is not necessary to track an object through a dynamic scene, but just to determine when an object reaches a vertex, which is generally easier than estimating a continuous trajectory.

#### 3.1 Problem Solving

More formally, let  $X_{j,t}$ ,  $j = 1, \dots, c$ , be the quantity of “transmitted” fluorescence on the OD pair  $j$  at time  $t$ . The measurements  $\mathbf{Y}_t = (Y_{1,t}, \dots, Y_{r,t})^T$  are computed as explained in Section 2. The inherent randomness of the measurements motivates the adoption of a statistical approach. Now, we reasonably assume that the whole traffic is temporally distributed as a Poisson process,  $X_{j,t} \sim \text{Poisson}(\lambda_j)$ . In this traffic flow problem, we then assume the following model:

$$\mathbf{Y}_t = \mathbf{A}\mathbf{X}_t, \quad (2)$$

where  $\mathbf{X}_t = (X_{1,t}, \dots, X_{c,t})^T$ , and  $\mathbf{A}$  denotes a  $r \times c$  routing matrix which binary elements  $A_{ij} = 1$  if edge  $i$  is in the path for the OD pair  $j$ , and 0 otherwise.

For illustration, if we consider the simple example shown in Fig. 3, some rows of the matrix  $\mathbf{A}$  are presented in Tab. 4. Typically, the number  $c$  is greater than  $r$ , and the problem is then under-constrained. Additional constraints are necessary for solving this inverse problem. First, (Vardi, 1996) proposed to introduce constraints related to the assumption that the traffic is temporally Poisson distributed. The NT method amounts then to estimating the values  $\lambda_j$  given the additional set of equations corresponding to temporal averages:

Table 4: Part of the matrix  $\mathbf{A}$  corresponding to the graph shown in Fig. 3.

OD pairs	edges					
	1	2	3	4	5	6
1 → 2	0	1	0	0	0	0
1 → 3	0	0	0	0	1	0
1 → 4	0	0	1	0	0	0
2 → 1	1	0	0	0	0	0
2 → 3	1	0	0	0	1	0
2 → 4	1	0	1	0	0	0
...	...					

$$\begin{cases} \bar{Y}_i = \sum_{k=1}^c A_{i,k} \lambda_k, & i = 1, \dots, r, \\ \text{cov}(Y_i, Y_{i'}) = \sum_{k=1}^c A_{i,k} A_{i',k} \lambda_k, & 1 \leq i \leq i' \leq r. \end{cases}$$

This set of equations gives a system of  $r(r+3)/2$  linear equations that forms an over-constrained problem that can be better solved with the conditions  $\lambda_i \geq 0$ . Moreover, in this application, the aim is not to obtain the number of vesicles that utilize each path, but to estimate the proportions of vesicles on each path. Hence, unlike previous methods (Vardi, 1996; Santini, 2000; Boyd et al., 1999), we impose the condition  $\sum_{i=1}^c \lambda_i = 1$  as an additional constraint. The previous system can be written more compactly as:

$$\begin{pmatrix} \bar{\mathbf{Y}} \\ \mathbf{S} \end{pmatrix} = \begin{pmatrix} \mathbf{A} \\ \mathbf{B} \end{pmatrix} \Lambda, \quad (3)$$

where  $\Lambda = (\lambda_1, \dots, \lambda_c)^T$  contains the temporal mean of the traffic flow,  $\mathbf{S} = \{\text{cov}(Y_i, Y_{i'})\}$  is the sample covariance matrix rewritten as a vector of length  $r(r+1)/2$ , and  $\mathbf{B}$  is an  $(r(r+1)/2) \times c$  matrix with the  $(i, i')$ th row of  $\mathbf{B}$  being the element-wise product of row  $i$  and row  $i'$  of the matrix  $\mathbf{A}$ .

The system can be solved using the estimation-maximization (EM) method (Vardi, 1996; Santini, 2000) or the convex-projection algorithms (Boyd et al., 1999). In our case, we adapt a non negative mean square estimation which also provides a simple and reliable way to estimate the OD traffic  $\hat{\Lambda}$ . For the implementation, our method is based on the *lsqnonlin* function from the Matlab Optimization toolbox. Note that a review of existing methods is also proposed in (Medina et al., 2002).

#### 3.2 Origin-destination Regions Partially Known

When the expert specifies the origin or destination regions, the problem is better constrained and the solu-

tion is expected to be more relevant.

Typically, if we assume that the origins or destinations for the regions are known, this can be casted into additional hard constraints. If the Voronoi cell  $r$  is the single origin region, then all the OD pairs that have another Voronoi cell than  $r$  as origin have no longer meaning. So all that OD pairs can be ignored. Hence, let  $\mathcal{R}$  be all the OD pairs that have  $r$  for origin. Then, if  $\mathcal{O}$  denotes the set of all OD pairs,  $\mathbf{A}$  can be modified as

$$\mathbf{A}(:, \mathcal{O} \setminus \mathcal{R}) = 0,$$

with  $\mathbf{A}(:, \mathcal{O} \setminus \mathcal{R}) = \{\mathbf{A}(1, \mathcal{O} \setminus \mathcal{R}); \mathbf{A}(2, \mathcal{O} \setminus \mathcal{R}); \dots; \mathbf{A}(r, \mathcal{O} \setminus \mathcal{R})\}$ . The same modeling can be applied for imposing additional origin or destination regions.

## 4 EXPERIMENTAL RESULTS

In this section, we propose three experiments to demonstrate the ability and the limits of the NT-based approach applied to a real image sequence. All these experiments are tested by considering the sequence shown in Fig. 1. This sequence is composed of 900 images coming from a fast 4D deconvolution microscopy (wide-field) process (Sibarita et al., 2006). In this sequence, the background was removed during a preprocessing step. The estimated results are reported in Figs. 6 and 7. In these figures, the Voronoi cells are represented in red, while the MIP map is shown in the background by transparency. The different estimated OD pairs appear as colored arrows, and the corresponding colored numbers at the right top of the figures are the estimated proportions of moving vesicles for each OD pair.

A first experience was carried out with a crude segmentation, without imposing origin or destination regions. The results are shown in Fig. 6 (left). According to the expert-biologists, the vesicles are moving from the Golgi Apparatus (the central region) to end-points located at the periphery of the cell (corresponding to the three other regions). But, in this experience, the traffic is estimated going from end-points to end-points, which is not consistent with prior knowledge. That is why we impose, in a second experiment, (Fig. 6, right image), the central region to be the origin Voronoi cell. The results obtained with this additional constraint correspond to trafficking from the Golgi Apparatus to the end-points. In that case, the traffic tends to be quite uniform for all the end-points.

In another experiment corresponding to another partition of the image shown in Fig. 7 (left), the previous central Voronoi cell is divided into several cells,

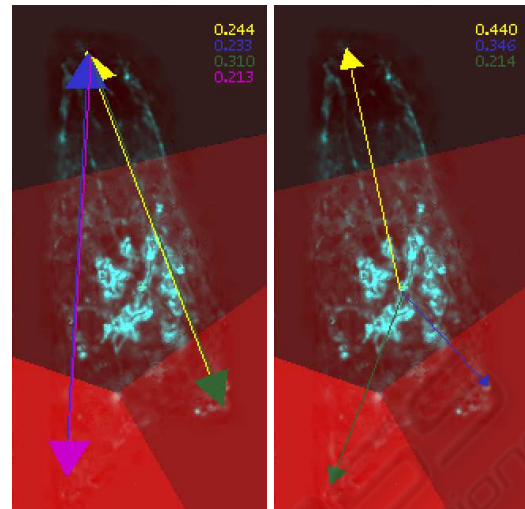


Figure 6: Results obtained by applying the NT-based approach on the sequence of the Fig. 1. The arrows represent the estimated OD pairs, and the corresponding colored numbers at the top right represent traffic proportions. Left: no origin region is imposed; right: the central region is imposed to be an origin region.

and they are all constrained to be origin regions. The estimated traffic from these origin regions to the end-points corresponds to proportions similar to proportions estimated in the previous experiment. In addition, the estimated traffic seems to be isotropic, i.e. there is no particular directions for traffic.

Finally, an experience is conducted with the same constrained origin region than the first experiment, but with one more end-point at the top of the image, and with intermediate Voronoi cells between the origin and the destinations (Fig. 7, right). Although the destination cells are not labeled, the whole trafficking is estimated from the Golgi Apparatus to the end-points. In addition, the sum of estimated proportions of the traffic towards the two regions at the top of the image is quite similar to the estimated proportions of the traffic towards the region at the top of the image in the first experiment. However, the estimated proportions of traffic towards the regions located at the bottom of the image are different from the estimated proportions of traffic towards the same regions in the first experience.

## 5 CONCLUSIONS

In this paper, we propose several contributions: *i*) definition of a graph by partitioning the image using a Voronoi diagram; *ii*) temporal estimation of moving vesicles; *iii*) application of the NT concept to real image sequences. The results obtained on the real image

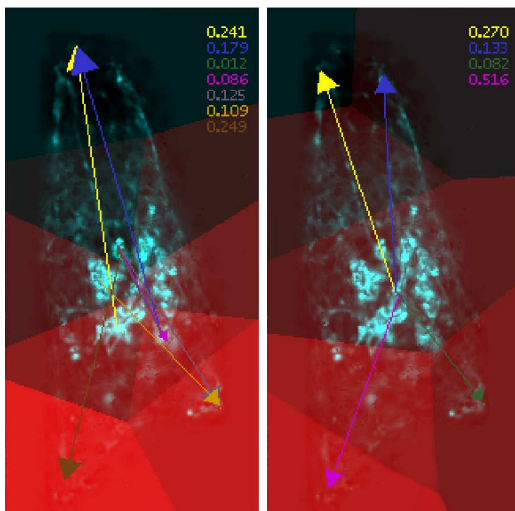


Figure 7: Results obtained by applying the NT-based approach on the sequence of Fig. 1. The arrows represent the estimated OD pairs, and the corresponding colored numbers at the top right represent traffic proportions. Left: all the central regions are imposed to be origin regions; right: the central region is imposed to be an origin region.

sequence suits the biological knowledge about the OD regions for the Rab6 trafficking. In our experiments, the proportions of vesicles for the OD pairs given by the NT procedure represent new tools for biologists. It can be applied to understand other trafficking problems where many objects are moving. Actually, the main limit is related to image partition yet, which can be arbitrary. Indeed, although the expert defines the centers of Voronoi cells with biological knowledge, the segmentation remains very crude for representing the regions of interest. Actually, the MIP map is the only tool available to define these regions, but is not enough accurate. For future work, it will be necessary to apply the NT-based approach on more relevant regions. A possible way is to extract the microtubule network and consider it as a graph for applying the NT procedure. Moreover, it is established that the fluorescence decreases with time, which is neglected in our modeling since we exploit the difference of fluorescence between two time steps. However, it is well known that the vesicles diffuse also in the cytosol. This could be considered in future work by introducing this phenomenon in the estimation process of the data to improve the results.

## REFERENCES

Anderson, C., Georgiou, G., Morrison, I., Stevenson, G., and Cherry, R. (1992). Tracking of cell surface receptors by fluorescence digital imaging microscopy

using a charged-coupled device camera. low-density lipoprotein and influenza virus receptor mobility at 4 degrees c. *Journal of Cell Science*, 101:415–425.

Barber, C., Dobkin, D., and Huhdanpaa, H. T. (1996). The quickhull algorithm for convex hulls. *ACM transactions on mathematical software*, 22(4):469–483.

Bechar, I. and Trubuil, A. (2006). A bidimensional signal processing approach to vesicle trafficking analysis in 3d+t fluorescence videomicroscopy. *Proc. of the MICCAI Workshop on Microscopic Image Analysis and Application to Biology*.

Boulanger, J., Kervrann, C., and Bouthemy, P. (2006). Estimation of dynamic background for fluorescence video-microscopy. In *Proc. of ICIP'2006*, Atlanta.

Boyd, J. E., Meloche, J., and Vardi, Y. (1999). Statistical tracking in video traffic surveillance. In *Proc. of ICCV'99*, volume 1, pages 163–168.

Candes, E. and Tao, T. (2007). The dantzig selector: statistical estimation when  $p$  is much larger than  $n$ . *Annals of statistics*, to appear.

Medina, A., Taft, N., Salamatian, K., Bhattacharyya, S., and Diot, C. (2002). Traffic matrix estimation: existing techniques and new directions. In *SIGCOMM '02: Proc. Conf. on Applications, Technologies, Architectures, and Protocols for Computer Communications*, pages 161–174, New York, USA.

Pécot, T., Boulanger, J., Kervrann, C., and Bouthemy, P. (2007). Network tomography for trafficking simulation and analysis in fluorescence microscopy imaging. In *Proc. of IEEE ISBI'2007*, pages 268–271, Arlington.

Racine, V., Hertzog, A., Jouaneau, J., Salamero, J., Kervrann, C., and Sibarita, J. (2006). Multiple target tracking of 3d fluorescent objects based on simulated annealing. In *Proc. of IEEE ISBI'2006*.

Santini, S. (2000). Analysis of traffic flow in urban areas using web cameras. In *Fifth IEEE Workshop on Applications of Computer Vision*, volume 596, pages 140–145.

Sbalzarini, I. and Koumoutsakos, P. (2005). Feature point tracking and trajectory analysis for video imaging in cell biology. *Journal of Structural Biology*, 151:182–195.

Sibarita, J., Racine, V., and Salamero, J. (2006). Quantification of membrane trafficking on a 3d cytoskeleton network in living cells. In *Proc. of IEEE ISBI'2006*.

Smal, I., Niessen, W., and Meijering, E. (2007). Advanced particle filtering for multiple object tracking in dynamic fluorescence microscopy images. In *Proc. of IEEE ISBI'2007*, pages 1048–1051, Arlington.

Thomann, D., Dorn, J., Sorger, P., and Danuser, G. (2003). Automatic fluorescent tag localization ii: improvement in super-resolution by relative tracking. *Journal of Microscopy*, 211(3):230–248.

Tibshirani, R. (1996). Regression shrinkage and selection via the lasso. *Journal of the Royal Statistical Society*, 58:267–288.

Vardi, Y. (1996). Network tomography: Estimation of source-destination traffic intensities from link data. *Journal of the American Statistical Association*, 91(433):365–377.